Zhong et al. *Zool. Res.* 2026, 47(1): 289−302
https://doi.org/10.24272/j.issn.2095-8137.2025.143
https://cstr.cn/32248.14.zr.2025.143

ZR | Zoological Research

Article Open Access

Phylogenomic analysis of Cervidae provides insights into antler origin and evolution

Zhenyu Zhong[1,9,#], Zihe Li[2,#], Zhili Zuo[3,#], Quanmin Zhao[4,#], Zhipeng Li[5,#], Bao Wang[2,#], Botong Zhou[2], Qingyun Guo[1,9], Zhibin Cheng[1,9], Jie Mao[3], Huishan Yue[2], Wenbo Zhu[2], Ge Han[2], Yusu Wang[4], Guifen Zhou[6], Lei Chen[2], Michael V. Westbury[7], Qiang Qiu[2], Rasmus Heller[8,*], Wen Wang[2,*], Lisen Li[2,*]

[1] *Beijing Milu Ecological Research Center*, *Beijing* 100076, *China*
[2] *New Cornerstone Science Laboratory*, *Shaanxi Key Laboratory of Qinling Ecological Intelligent Monitoring and Protection*, *School of Ecology and Environment*, *Northwestern Polytechnical University*, *Xi'an*, *Shaanxi* 710072, *China*
[3] *Chengdu Zoo (Chengdu Wildlife Research Institute)*, *Chengdu*, *Sichuan* 610081, *China*
[4] *College of Chinese Medicinal Materials*, *Jilin Agricultural University*, *Changchun*, *Jilin* 130118, *China*
[5] *College of Animal Science and Technology*, *Jilin Agricultural University*, *Changchun*, *Jilin* 130118, *China*
[6] *College of Engineering and Technology*, *Jilin Agricultural University*, *Changchun*, *Jilin* 130118, *China*
[7] *GLOBE Institute*, *University of Copenhagen*, *Copenhagen DK*-1350, *Denmark*
[8] *Section for Computational and RNA Biology*, *Department of Biology*, *University of Copenhagen*, *Copenhagen DK*-2100, *Denmark*
[9] *National Conservation and Research Center for Milu*, *Beijing* 100076, *China*

ABSTRACT

Antlers represent the only known example of complete annual organ regeneration in mammals. Despite this unique regenerative capacity, the genetic mechanisms driving antler origin and morphological diversification across Cervidae remain poorly understood. This study assembled six high-quality chromosome-level genomes of cervids spanning four distinct tribes, including the first genomic reference for the tufted deer (*Elaphodus cephalophus*). Comparative analyses across the Cervidae lineage identified signatures of positive selection on gene networks governing stem cell differentiation and bone metabolism, with elevated expression of these genes detected in antler developmental and regenerative tissues. Tribe-specific selective pressures in Cervini and Odocoileini further revealed convergent evolution targeting core developmental pathways, notably the RAS/MAPK pathway, implicating these pathways in both the emergence and enhancement of antler traits. In contrast, relaxed selective constraints in the antlerless Chinese water deer (*Hydropotes inermis*) revealed disruptions in gene modules associated with tumor suppression and skeletal homeostasis, suggesting a rewiring of regulatory homeostasis. These findings highlight how antler evolution reshaped physiological trade-offs, including reduced oncogenic susceptibility and enhanced tissue regeneration and cyclic bone remodeling. This study advances current understanding of antler evolution and diversification, while providing genomic resources for mammalian regenerative biology.

Keywords: Cervidae; Telomere-to-telomere genome assembly; Origin and evolution of antlers; Physiological rewiring associated with antlers

INTRODUCTION

Antlers constitute the only known example of complete and cyclical organ regeneration in mammals, functioning not only as dynamic osseous structures but also as key indicators of sexual selection and social hierarchy in cervids (Cegielski et al., 2006; Clutton-Brock et al., 1982, 1988; Kruuk et al., 2002; Malo et al., 2005; Suttie, 1980; Wang et al., 2019a). The extraordinary characteristics of cervid antlers prompted the late developmental biologist Richard Goss of Brown University to remark that "The antlers of cervids are so improbable that if they had not evolved in the first place, they would never have been conceived even in the wildest fantasies of the most imaginative biologists" (Goss, 1983). Despite their striking

Received: 14 June 2025; Accepted: 10 September 2025; Online: 11 September 2025

Foundation items: This work was supported by the National Natural Science Foundation of China (32388102, 32030016, 32220103005) and New Cornerstone Investigator Program to W.W., Financial Program of BJAST (11000025T000003328806) to Z.Y.Z., National Natural Science Foundation of China (32122083) to Z.P.L., and China Postdoctoral Science Foundation (2024M764241) to L.S.L.

[#]Authors contributed equally to this work

*Corresponding authors, E-mail: rheller@bio.ku.dk; wenwang@nwpu.edu.cn; lisenli@nwpu.edu.cn

phenotypes, antler morphology does not strictly reflect phylogenetic relationships across Cervidae. While traditionally divided into four subfamilies—Cervinae, Odocoileinae, Muntiacinae, and Hydropotinae (Wilson & Reeder, 1993)—recent mitochondrial phylogenies have reclassified the clade into four tribes: Cervini and Muntiacini within a revised Cervinae, Odocoileini and Capreolini within Capreolinae (Gilbert et al., 2006; Jiang et al., 2023; Zhang & Zhang, 2012). Cervini and Odocoileini exhibit more elaborate trifurcated antlers, whereas their sister tribes, Muntiacini and Capreolini, possess reduced or unbranched antlers. Notably, Capreolini includes the Chinese water deer (*Hydropotes inermis*), which lacks antlers entirely (Samejima & Matsuoka, 2020). To date, the genetic mechanisms underlying antler origin and evolution remain largely unresolved. Additionally, intriguing evolutionary questions persist in Cervidae, such as extreme karyotypic remodeling during the radiation of Muntiacini (Zhang et al., 2021b). This tribe comprises two genera, *Elaphodus* (tufted deer) and *Muntiacus* (muntjacs), which exhibit markedly reduced chromosome counts compared to the ancestral cervid karyotype of 2*n*=70 (Huang et al., 2006). Notably, the tufted deer (*Elaphodus cephalophus*), the monotypic genus in Muntiacini, contains a chromosome number of 2*n*=48, while that of the Reeves' muntjac (*Muntiacus reevesi*) is 2*n*=46, raising questions regarding whether this similarity reflects shared ancestry or convergent chromosomal fusion events. Comparative analyses of genomic synteny may help elucidate whether *Elaphodus* retained an ancestral karyotype or underwent independent fusion events parallel to those in *Muntiacus*. Palindromic repeat sequences, known to induce double-strand breaks, have been identified flanking the short telomeric sequences in *Muntiacus* genomes, which may act as drivers of prolific chromosomal fusions (Yin et al., 2021). However, whether these palindromic structures are a synapomorphic feature of Muntiacini or unique to *Muntiacus* has yet to be clarified.

Cervid antler regeneration represents one of the fastest known rates of organogenesis among mammals, with growth rates up to 2.75 cm per day (Landete-Castillejos et al., 2019; Price et al., 2005). This extreme growth demands substantial metabolic resources and triggers the activation of proto-oncogenes associated with proliferative signaling (Wang et al., 2019c). Despite the theoretical increase in oncogenic risk, tumor suppressor pathways appear to be under strong evolutionary constraint, potentially explaining the exceptionally low incidence of spontaneous malignancies in cervid populations (Lombard & Witte, 1959; Wang et al., 2019c). Notably, recent research has demonstrated antineoplastic effects of proliferating antler tissue extracts against human tumor cells, further implicating active cancer surveillance mechanisms during antlerogenesis (Rossetti et al., 2024). Additionally, the significant calcium demands of rapid osteogenesis during antler regeneration induce systemic skeletal remodeling. Reports have documented seasonal mobilization of calcium from other skeletal bones, followed by post-regenerative replenishment, a process manifesting as annual cyclic physiological osteoporosis (Banks et al., 1968; Stéger et al., 2010). To date, however, the genetic basis of these coordinated physiological changes remains poorly defined. Expanding the availability of high-quality genome assemblies across phylogenetically diverse lineages will facilitate integrative phylogenomic analyses aimed at uncovering the evolutionary genetic basis of these unique traits.

Despite recent advances, high-quality genome assemblies in Cervidae remain sparse and unevenly distributed, limiting evolutionary and comparative genomic resolution. Earlier cervid genomes were assembled using diverse sequencing platforms: PacBio CLR for white-tailed deer (*Odocoileus virginianus*), mule deer (*Odocoileus hemionus*), and sika deer (*Cervus nippon*) (London et al., 2022; Lamb et al., 2021; Xing et al., 2023); Oxford Nanopore for Reeves' muntjac, Gongshan muntjac (*Muntiacus gongshanensis*), and Chinese water deer (Yin et al., 2021); and short-read, next-generation sequencing for reindeer (*Rangifer tarandus*) and roe deer (*Capreolus capreolus*) (Chen et al., 2019).However, these earlier cervid genome datasets are frequently limited by elevated error rates or incomplete assemblies, and, critically, no genome is currently available for the tufted deer. This absence, combined with the limited genomic representation of Cervini—the most species-rich tribe within Cervidae—hinders robust evolutionary inference and increases the risk of misidentifying stochastic polymorphisms as lineage-specific signals. Generating high-quality genomes from key lineages across the cervid phylogeny is essential for reducing such errors and enabling fine-scale comparative analyses of genetic divergence. In the case of giraffes, for example, the inclusion of additional high-quality ruminant genomes has helped resolve previously reported false-positive lineage-specific mutations (Liu et al., 2021). Recent advances in long-read sequencing have yielded high-fidelity genome assemblies for red deer (*Cervus elaphus*) (Pemberton et al., 2021), fallow deer (*Dama dama*) (Barnard et al., 2023), and sika deer (Li et al., 2025) using PacBio HiFi technology, marking a major step toward resolving these gaps.

This study generated high-quality chromosome-level genome assemblies for six cervid species using PacBio HiFi long-read sequencing combined with Hi-C chromosome conformation capture technologies. The species span four major tribes, including the tufted deer from Muntiacini; red deer, fallow deer, and hog deer (*Axis porcinus*) from Cervini; reindeer from Odocoileini; and Chinese water deer from Capreolini. To investigate population dynamics, additional 150 bp paired-end short-read data (insert size: 350 bp) were generated for all six species, four of which—tufted deer, hog deer, reindeer, and Chinese water deer—are currently classified as Near Threatened or higher on the IUCN Red List. For comparative and phylogenomic analyses, the dataset was expanded to include four recently published cervid genomes (sika deer, white-tailed deer, Reeves' muntjac, and Père David's deer (*Elaphurus davidianus*)), alongside outgroup taxa comprising the giraffe (*Giraffa camelopardalis rothschildi*), cattle (*Bos taurus*), goat (*Capra hircus*), and forest musk deer (*Moschus berezovskii*). These analyses revealed extensive chromosomal fusions within Muntiacini and uncovered the genetic mechanisms underlying antler evolution and broader physiological adaptations in cervids.

MATERIALS AND METHODS

Sample and data collection

Peripheral blood samples were obtained from red deer, fallow deer, Chinese water deer (Milu Park, Beijing, China), hog deer and tufted deer (Chengdu Zoo, Sichuan Province, China), and reindeer (Lushengyuan Animal and Plant Garden, Jilin Province, China). Approximately 10 mL of peripheral blood

was drawn from each individual and stored in EDTA-anticoagulation tubes at −80°C. In addition, antler buds (*n*=3) were collected from 150-day-old sika deer provided by Jilin Agricultural University for transcriptomic sequencing. All animal procedures complied with relevant ethical regulations and were approved by the Northwestern Polytechnic University Ethics Committee Institutional Review Board (Approval No. 202201015).

Genome assemblies generated using long-read sequencing platforms (PacBio or Oxford Nanopore), along with reference annotations for human (*Homo sapiens*) (hg38; GCF_000001405.40), giraffe (GCA_017591445.1), goat (GCF_001704415.1), cattle (GCF_002263795.1), forest musk deer (GCA_022376915.1), white-tailed deer (GCA_014726795.1), Père David's deer (PRJNA438286), sika deer (GCA_038088365.1), and Reeves' muntjac (PRJNA640966), were downloaded from the NCBI database (https://www.ncbi.nlm.nih.gov/) for comparative genomic analyses.

Genomic DNA extraction

Genomic DNA was extracted using the cetyltrimethylammonium bromide (CTAB) method, followed by purification with the QIAGEN® Genomic Kit (Cat#13343, Qiagen, Germany), according to the standard operating procedures provided by the manufacturer. DNA quality was initially assessed by electrophoresis on 1% agarose gels to detect degradation and contamination. Purity was measured using a NanoDrop One UV-Vis spectrophotometer (Thermo Fisher Scientific, USA), with acceptable OD260/280 values between 1.8 and 2.0 and OD 260/230 values between 2.0 and 2.2. DNA concentration was quantified using a Qubit® 4.0 fluorometer (Invitrogen, USA).

Library preparation and sequencing

High-molecular-weight DNA libraries (*n*=6), representing red deer, fallow deer, tufted deer, reindeer, hog deer, and Chinese water deer, were constructed for PacBio HiFi sequencing according to the manufacturer's protocols (Pacific Biosciences, USA). Libraries with an average insert size of 15 kb were sequenced on the PacBio Sequel II platform at approximately 30× coverage using three SMRT cells per species. Hi-C libraries were constructed and sequenced for all six species to a depth of approximately 100× (250 Gbp) to scaffold contigs into chromosome-level assemblies. In addition, short-read sequencing (50×, 125 Gbp) was performed on the DNBSEQ-T7 sequencing platform to generate data for subsequent PSMC analysis. Genome assembly was conducted using Hifiasm (v.0.19.5) with the following parameters: "hifiasm -o prefix of output files -t 30 file names of HiFi --h1 file names of Hi-C R1 --h2 file names of Hi-C R2 2> out.log". Contigs were scaffolded into chromosome-level assemblies using Juicer and 3D-DNA pipelines (Dudchenko et al., 2017; Durand et al., 2016). Briefly, HiFi and Hi-C reads were used to obtain non-redundant haplotype-resolved contigs and haplotype-phased pseudo-autosomal region (PAR) sequences of the X and Y chromosomes. Subsequently, Hi-C data were used to generate chromosome-level assemblies, including X and Y chromosomes. Assembly completeness was evaluated using BUSCO (v.4.0.2) (Waterhouse et al., 2018) with the certa_odb10 database and the following parameters "busco -i HiFi.fasta -c 100 -m geno -o busco.out -l certa_odb10 --offline". For genomic annotation, transcriptomic sequencing (10 Gbp per species) was performed as described previously (Chen et al., 2018). Repetitive elements were identified and masked using RepeatMasker (v.4.1.0) (Tarailo-Graovac & Chen, 2009).

Phylogenetic analysis

Phylogenetic reconstruction was performed using both concatenation-based and coalescence-based approaches across two independent datasets. The first dataset consisted of a 1.5 Gb multi-genome alignment generated for 14 species using Cactus (Armstrong et al., 2020). A guide tree for Cactus was constructed from annotated protein sequences using OrthoFinder (v.2.5.5) (Emms & Kelly, 2019) with the parameters "-M msa -T iqtree". Aligned genomic sequences were extracted and concatenated to construct a species tree with IQ-TREE2 (v.1.6.12) (Minh et al., 2020), using the parameters "-B 1000 -T 96 -alrt 1000 -m GTR+F+R6". To refine phylogenetic signal, alignment blocks located within at least 2 kb of single-copy, repeat-free regions were extracted using "hal2maf" in the HAL package (Hickey et al., 2013), with uninformative gaps trimmed using trimAl with the parameter "automated1" (Capella-Gutiérrez et al., 2009). Single-copy regions were identified using 'halSingleCopyRegionsExtract' from the Cactus package, and overlapping repetitive elements were filtered using BEDTools based on annotations from the sika deer genome. Blockwise phylogenies were constructed for each alignment segment using IQ-TREE with the parameter "-m GTR+F+R6", and a coalescent-based species tree was then inferred using ASTRAL-III (v.5.7.1) (Zhang et al., 2018), following the framework described in Feng et al. (2022).

The second dataset contained 16 827 synteny-defined protein-coding orthologous gene families across 14 species, including 10 cervids from all four subfamilies and four outgroups (giraffe, cattle, goat, and forest musk deer). Genomes were first aligned to the human reference (hg38) using SegAlign (Goenka et al., 2020), and syntenic chains were extracted using the UCSC chainNet pipeline (2024 update) (Raney et al., 2024). Orthologous and lost genes were identified with TOGA (Kirilenko et al., 2023). Single copy orthologs were extracted using "extract_codon_alignment.py" in TOGA, and codon-aware alignments were generated using MACSE2 (Ranwez et al., 2018). A total of 3 585 992 four-fold degenerate sites were extracted using a custom Perl pipeline (https://github.com/yongzhiyang2012/genome_analysis/tree/master/evolution/02.phylogenetic) and concatenated for tree construction using IQ-TREE2, with the parameters "-B 1000 -alrt 1000 -m GTR+F+R6". Divergence times were estimated using MCMCTREE (Yang, 2007), with fossil calibrations applied to Cervidae (8.5–17.7 million years ago (Ma)) and the ancestor of Bovidae and Moschidae (17.65–26.1 Ma). Phylogenetic trees for each protein-coding ortholog gene family were inferred using IQ-TREE2 with the parameters "-seqtype CODON -m GY+F3X4+I+G", and ASTRAL-III (v.5.7.1) was used to generate a coalescent species tree (Zhang et al., 2018). To further investigate genome-wide synteny, MCScanX (Wang et al., 2012) was used with default parameters to identify collinear blocks among cattle, red deer, fallow deer, reindeer, and Chinese water deer, with cattle selected as the reference outgroup due to the availability of a high-quality chromosome-level genome and well-curated annotations (Yin et al., 2021). Chromosome-scale syntenic block plots were constructed using SynVisio (Bandi & Gutwin, 2020). Finally, phylogenetic discordance was assessed using DiscoVista (v.1.0) and relative frequency analysis (Sayyari et al., 2018) to

quantify alternative branching (discordance) among phylogenies.

Satellite and telomeric sequence content in HiFi reads

Satellite and telomeric sequence content was analyzed in tufted deer, sika deer, reindeer, and Chinese water deer, following previously described methods (Yin et al., 2021). Briefly, based on fusion sites reported in previous research on muntjac species, monomer sequences representing three satellite classes (satI, satII, and satIV) identified in the female black muntjac (*Muntiacus crinifron*) genome (Yin et al., 2021), along with vertebrate telomeric repeats ((TTAGGG)n), were aligned to the HiFi reads of fallow deer, hog deer, red deer, tufted deer, sika deer, reindeer, and Chinese water deer using BLAST (-evalue 0.001) (Camacho et al., 2009). Reads containing these motifs were then classified into distinct patterns and quantified, as described in a previous study (Yin et al., 2021). To identify palindromic structures, self-BLAST analyses were conducted on reads containing satellite and telomeric sequences (Camacho et al., 2009). Reads with coverage≤2 were regarded as sequencing errors and excluded from downstream analyses (Kelley et al., 2010).

Demographic analysis

Short-read data (approximately 50× coverage) generated on the DNBSEQ-T7 platform were subjected to adapter trimming and quality filtering using Fastp (Chen et al., 2018). Filtered reads were mapped to the respective reference genome using BWA-MEM. BCFtools (Danecek et al., 2021) was used to call single nucleotide polymorphisms (SNPs). Variants with depth <30× or >200×, as well as those located on sex chromosomes, were excluded using "vcfutils.pl". Demographic history was inferred with PSMC (Li & Durbin, 2011) using the following parameters: psmc -N25 -t15 -r5 -b -p 4+25*2+4+6. Generation times for each species were obtained from the IUCN Red List (https://www.iucnredlist.org/), and mutation rates were estimated using MCMCTREE based on the four-fold degenerate site-based concatenated phylogenetic tree. The generation times applied were as follows: red deer, 7 years (Hoffmann et al., 2016); fallow deer, 1 year (Baker et al., 2017); tufted deer, 2 years (Sun et al., 2016); reindeer, 6 years (Kvalnes et al., 2024); hog deer, 5 years (Ramsey et al., 2019); and Chinese water deer, 5 years (Chen et al., 2019).

Identification of positively selected genes (PSGs)

Lineage-specific evolutionary rates were estimated using the Codeml program in the PAML package (v4.8) (Yang, 2007). The branch-site model was applied to detect PSGs. To identify selection associated with antler origin, the Cervidae lineage was designated as the foreground branch, while all cervids and outgroup species were treated as the background branch. To examine evolutionary changes linked to more elaborate antlers, Cervini and Odocoileini were defined as the foreground branches, with the remaining cervids as background. Likelihood ratio tests (LRTs) were performed to compare the alternative model allowing codons with ω>1 against a null model constrained to ω≤1, using chi-square statistics implemented in PAML (Yang, 2007). Posterior probabilities of positive selection at specific codon sites were inferred using the Bayes Empirical Bayes (BEB) approach under the M2A model. Genes were classified as significant PSGs if LRT *P*-values were <0.05 and BEB posterior probabilities exceeded 0.95, while those with probabilities >0.5 were considered moderate PSGs. The free-ratio model within Codeml was used to calculate gene-wise dN/dS ratios as a measure of evolutionary rate variation. For significant PSGs, AlphaFold2 (Jumper et al., 2021; Mirdita et al., 2022) was used to predict and visualize three-dimensional protein structures. To assess relaxed selection in Chinese water deer relative to other cervids, the RELAX method (Pond & Frost, 2005) implemented in HyPhy (Pond et al., 2005) was applied. Genes showing significant relaxation (P<0.05, k<1) were identified as undergoing reduced selective constraint in the Chinese water deer.

Gene family expansion analysis

For gene family analysis, the longest isoforms of annotated protein-coding genes were extracted for 14 target species, including giraffe, goat, cattle, forest musk deer, white-tailed deer, Père David's deer, sika deer, Reeves' muntjac, reindeer, hog deer, Chinese water deer, tufted deer, fallow deer, and red deer using AGAT (v.0.8.0) (Dainat, 2022) and GffRead (v.0.12.7) (Pertea & Pertea, 2020). Orthologous gene families were inferred using OrthoFinder (v2.5.5) (Emms & Kelly, 2019) with default parameters. Gene family expansions and contractions along the phylogenetic tree were estimated using CAFÉ (v.4.2.1) (De Bie et al., 2006). Families showing significant change across the entire tree and at specific nodes (P<0.05) were treated as lineage-specific extractions or expansions.

RNA sequencing (RNA-seq) and single-cell RNA-seq (scRNA-seq) data collection and analysis

Bulk RNA-seq data for sika deer antler bud were generated using the Illumina NovaSeq 6000 platform and deposited in the China National Center for Bioinformation (CNCB) under accession number CRA022995. RNA-seq data for sheep horn bud were retrieved from a previous study (Wang et al., 2019c) (PRJNA438286). To reduce annotation-related discrepancies between sika deer and sheep genomes, raw RNA-seq reads from both species were mapped to the sika deer reference genome using HISAT2 (v.2.2.1) (Zhang et al., 2021a) with the parameters "--very-sensitive --dta". The average mapping rate for sheep reads was 91.33%, indicating high compatibility and reliability for downstream analysis. Gene expression quantification was conducted using StringTie (v.2.1.7) (Pertea et al., 2015), and count matrices were generated via the prepDE.py script provided with the package. Differential expression analysis between antler and horn buds was carried out using the DEseq2 package, following standard procedures (Love et al., 2014). For scRNA-seq analysis, data from regenerating antler tissue were obtained from a previous study (Qin et al., 2023). Raw sequencing reads were processed with 10× Genomics Cell Ranger (v.8.0.1). Downstream normalization, dimensionality reduction, and visualization were performed in Scanpy, following a standardized pipeline (Li et al., 2025; Wolf et al., 2018).

Lineage-specific mutation and pathway analyses

Deduced amino acid sequences encoded by PSGs, along with specific site mutations across species, were aligned and visualized using AliView (Edgar, 2004). Protein family classification, domain prediction, and identification of functionally important residues were performed using InterPro (Paysan-Lafosse et al., 2023). Gene Ontology (GO) and Kyoto Encyclopedia of Genes and Genomes (KEGG) pathway analyses were performed using g:Profiler (Kolberg et al., 2023) and Enrichr (https://maayanlab.cloud/Enrichr/) (Chen

et al., 2013). Visualization of results was carried out using the Generic Diagramming Platform (https://BioGDP.com) (Jiang et al., 2025) and finalized in Inkscape (www.inkscape.org/).

RESULTS AND DISCUSSION

Chromosome-level genome assemblies and phylogenomic framework across Cervidae

PacBio HiFi, Hi-C, and paired-end short-read sequencing were performed for six cervid species representing all four major Cervidae tribes, including hog deer, red deer, and fallow deer from Cervini; tufted deer from Muntiacini; reindeer from Odocoileini; and Chinese water deer from Capreolini (Figure 1A) (CNCB, 2025a). After stringent filtering to remove low-quality and contaminant sequences, between 4 200 845 and 7 228 228 high-precision long reads were retained, with average read lengths ranging from 16 091.30 to 17 940.20 bp (Supplementary Table S1). The resulting assemblies spanned 3.0 to 3.5 Gb (Supplementary Table S1), exceeding the size of earlier cervid genomes (Chen et al., 2019; Yin et al., 2021) and closely aligning with the recently generated HiFi-based assembly of sika deer (Li et al., 2025). These expanded genome sizes likely reflect improved anchoring of complex repeat regions in pericentromeric and centromeric domains, enabled by the high-fidelity long-read data (Li et al., 2025). Repeat content constituted 36.55% to 44.34% of the assembled genomes, dominated by long interspersed nuclear elements (LINEs, 666.23–793.11 Mbp), short interspersed nuclear elements (SINEs, 157.16–280.11 Mbp), and satellite DNA (92.15–368.99 Mbp), with smaller contributions from long terminal repeats (LTRs, 93.37–122.11 Mbp) and DNA transposons (57.75–81.92 Mbp) (Supplementary Table S2). While LINE and SINE distributions were broadly consistent with previously reported cervid genomes (Han et al., 2023; Pemberton et al., 2021; Xing et al., 2023), the higher satellite DNA content suggests that HiFi-based genome assemblies offer higher resolution in centromeric regions, consistent with observations in *Arabidopsis* (Rabanal et al., 2022) and sika deer (Li et al., 2025). Merqury analysis (Rhie et al., 2020) yielded QV scores between 61.00 and 73.23 across species, corresponding to over 99.99% single-base accuracy. Assembly completeness was further supported by BUSCO scores ranging from 96.00% to 99.00%, short-read mapping rates between 93.64% and 98.46%, and contig N50 values between 34.18 and 65.04 Mbp. These chromosome-level genomes markedly increase the number of high-quality genomes in Cervini from three to five species and offer a robust genomic foundation for investigating the evolutionary diversification and lineage-specific innovations in antler development, chromosomal architecture, and ecological adaptation within Cervidae.

Using giraffe (Liu et al., 2021), cattle (Rosen et al., 2020), goat (Bickhart et al., 2017), and forest musk deer (Chen et al., 2022) as outgroups, multiple phylogenomic strategies were applied to reconstruct cervid evolutionary relationships. Whole-genome alignment of 14 species was performed using Cactus (Armstrong et al., 2020), yielding approximately 1.5 Gb of homologous sequences for phylogenetic inference (Figure 1A). To enhance phylogenetic resolution, repeat-overlapping regions and alignment blocks shorter than 100 bp were excluded. From the filtered dataset, 300 000 independent 1 kb repeat-free windows were selected to construct species trees using both concatenation-based and coalescent-based methods (Supplementary Figure S1A, B). A total of 16 827 orthologous protein-coding gene families were identified across the 14 species and used for separate species tree reconstructions through both concatenated alignments and gene tree reconciliation approaches (Supplementary Figure S1C, D). These trees exhibited highly consistent tribe-level topologies, with 100% bootstrap support and posterior probabilities of 1, aligning with the mitochondrial phylogeny previously reported by Jiang et al. (2023). These results provide the first genome-wide phylogenetic evidence confirming the placement of the tufted deer within Muntiacini. Within Cervini, however, topological discordance emerged. The concatenation-based tree constructed from orthologous gene alignments recovered the grouping of fallow deer and hog deer with moderate bootstrap support (84%) (Supplementary Figure S1C), in contrast to full support across other nodes. To further explore this uncertainty, the relative frequencies of different topologies were compared. Two configurations—t1 ((Père David's deer, hog deer), fallow deer) and t2 ((Père David's deer, fallow deer), hog deer) topologies—occurred at similar frequencies, both exceeding that of t3 ((fallow deer, hog deer), Père David's deer) (Supplementary Figure S2). This pattern is indicative of either incomplete lineage sorting or historical hybridization among these Cervini lineages.

Karyotypic restructuring frequently contributes to speciation and can profoundly influence genomic architecture and regulatory function (Eichler & Sankoff, 2003; Liu et al., 2021; Yin et al., 2021). Comparative analysis revealed that members of Odocoileini and its sister tribe Capreolini, including the Chinese water deer, retained the ancestral cervid karyotype of 2*n*=70 (Figure 1A), in agreement with prior cytogenetic studies (Hartmann & Scherthan, 2004; Wang & Lan, 2000; Yang et al., 1997). Within Cervini, multiple fusion events have reduced chromosome number, resulting in karyotypes of 2*n*=66 for sika deer and 2*n*=68 for Père David's deer, fallow deer, hog deer, and red deer (Figure 1A). In contrast, the karyotype of the tufted deer, the sole representative of *Elaphodus*, possessed a markedly reduced karyotype of 2*n*=48, consistent with earlier reports (Cao et al., 2005). Chromosome-level collinearity and centromere positioning traced 11 chromosomal fusion events underlying this karyotypic contraction in the tufted deer, including nine tandem fusions—linking the centromeric region of one ancestral chromosome to the telomeric end of another—and two Robertsonian fusions, formed by joining the proximal centromeric regions of two ancestral chromosomes. Only three tandem fusions were shared between tufted deer and Reeves' muntjac (Figure 1B; Supplementary Figure S3 and Table S3), indicating that most chromosomal fusions arose independently in the *Elaphodus* and *Muntiacus* lineages, as reported previously (Huang et al., 2006).

High-fidelity long-read sequencing of the tufted deer genome enabled precise resolution of telomeric and subtelomeric regions, revealing structural features implicated in lineage-specific chromosomal rearrangements. Previous analyses have implicated short telomeric repeats, flanking palindromic sequences, and associated Class I and IV satellite elements in driving extensive chromosomal fusions in Muntiacini (Yin et al., 2021). The new HiFi data refined these observations by correcting terminal sequencing errors and enabling high-confidence identification of telomeric architectures across cervids (Wu et al., 2024). Comparative

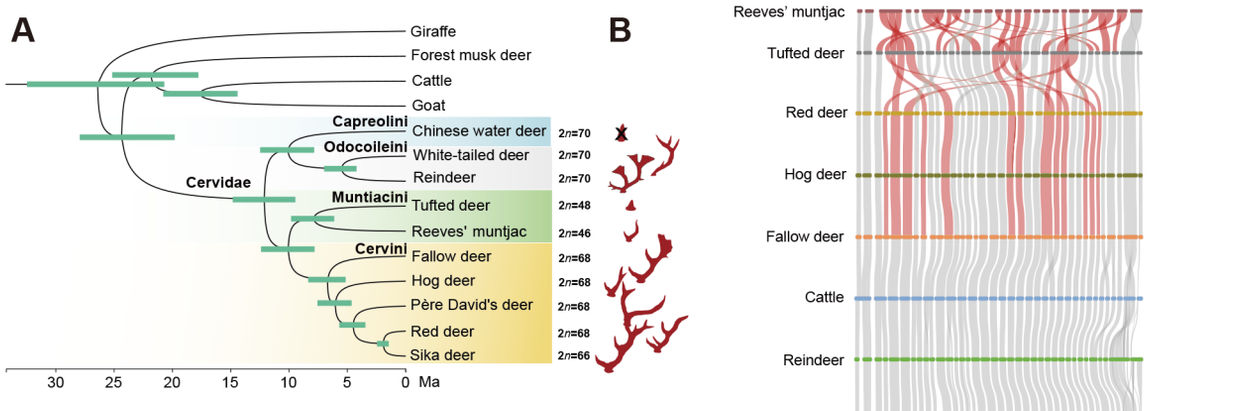

C

	satI-satIV-tel	Ratio (%)
Reeves' muntjac	2888	63.0
Gongshan muntjac	113	51.8
Black muntjac	450	74.3
Tufted deer	7	2.8
Fallow deer	3	1.2
Hog deer	0	0
Red deer	0	0
Sika deer	0	0
Reindeer	0	0
Chinese water deer	0	0

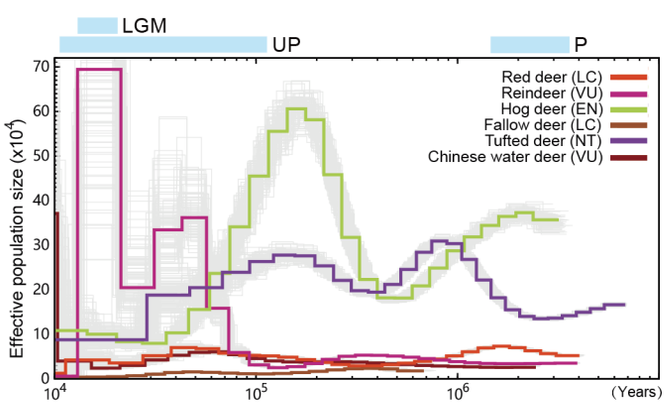

Figure 1 Evolutionary relationships and population dynamics of Cervidae

A: Whole-genome phylogeny of Cervidae reconstructed from 1.5 Gb of homologous sequences. Antler morphologies (Samejima & Matsuoka, 2020) and karyotypes are shown for each species. Ma: Million years ago. B: Chromosomal synteny among cattle, red deer, reindeer, tufted deer, Reeves' muntjac, hog deer, fallow deer, and Chinese water deer. Red ribbons indicate chromosomal fusion synteny blocks shared by tufted deer, Reeves' muntjac and members of the Cervini tribe. C: Abundance of reads containing satI-satIV-telomeric-repeat structures with palindromic sequences in tufted deer, fallow deer, hog deer, red deer, sika deer, reindeer, and Chinese water deer, along with previously reported data for Reeves' muntjac, Gongshan muntjac (*Muntiacus gongshanensis*), and black muntjac (Yin et al., 2021). Reads with sequencing coverage ≤2 were excluded as probable errors (Kelley et al., 2010). Percentages reflect the proportion of satellite-telomeric reads with palindromic repeats among all telomeric reads. D: Inferred demographic histories of six cervid species. Colored lines represent population size trajectories associated with different conservation statuses; light-colored lines represent 100 bootstrap replicates. Blue band represents geological time: Upper Pleistocene (UP); Last Glacial Maximum (LGM); Pliocene (P). IUCN categories: VU, vulnerable; EN, endangered; NT, near threatened; LC, least concern.

analysis across seven species representing all four tribes, including fallow deer, hog deer, red deer, sika deer, reindeer, tufted deer, and Chinese water deer, identified the recurrent presence of either satellite I and telomere (satI-telomere) or satellite IV and telomere (satIV-telomere) composite elements (Supplementary Figure S4). Notably, a more complex satI-satIV-telomere arrangement flanked by palindromic repeats was observed in the tufted deer, consistent with previous reports in muntjac species (Yin et al., 2021), and in fallow deer, the basal lineage within Cervini (Figure 1A). These findings suggest that palindromic satellite-telomere structures originated in the common ancestor of Cervinae (containing Cervini and Muntiacini) and subsequently underwent expansion in the ancestor of Muntiacini, leading to extensive chromosomal fusions in Muntiacini. Given recent progress in yeast and mouse models (Shao et al., 2018; Wang et al., 2022), the unique palindromic architectures found in Muntiacini may serve as valuable models for elucidating mechanisms of chromosomal instability and for advancing synthetic chromosome design.

Demographic reconstructions revealed divergent population trajectories among cervid lineages (Figure 1D). Species belonging to Muntiacini exhibited markedly greater historical effective population sizes (*Ne*) and more pronounced demographic fluctuations compared to other tribes prior to the Upper Pleistocene (129 000–11 700 years ago). Over the past 100 000 years, sharp *Ne* declines were detected in both tufted deer and hog deer, consistent with their classification as Endangered and Near Threatened by the IUCN (Smith et al., 2008; Sun et al., 2016). In contrast, reindeer exhibited a notable increase in *Ne* during the Last Glacial Maximum (26 500–19 000 years ago), likely reflecting population expansion in response to colder climatic conditions of the Late Pleistocene (Huybers & Wunsch, 2005; Locke, 1990), in line with previous research (Chen et al., 2019). Although elevated gene flow cannot be excluded as a contributing factor, the observed expansion supports the hypothesis that reindeer successfully adapted to high-latitude glacial environments. Following this peak, reindeer experienced a pronounced postglacial decline, paralleling the reduction in suitable habitat reported between 21 000 and 6 000 years before present (Lorenzen et al., 2011; Sommer et al., 2014), potentially

attributable to anthropogenic pressures and climate change. In comparison, the Chinese water deer exhibited a recent rise in *Ne* over the last 10 000 years, possibly reflecting demographic recovery or range expansion. Red deer and fallow deer, however, maintained relatively stable and consistently low *Ne* levels across this timeframe, underscoring the need for enhanced conservation attention for these less dynamically fluctuating lineages.

Genes associated with antler origin and evolution

To explore the genetic architecture underlying antler emergence, positive selection analyses were conducted across antler-bearing cervids, excluding the antlerless Chinese water deer to minimize signal dilution from relaxed selective constraint. This approach identified 152 PSGs within Cervidae (Figure 2A). Functional enrichment analyses revealed strong overrepresentation of pathways involved in stem cell differentiation, bone metabolism and remodeling, immune response, and signal transduction (Figure 2B). In parallel, 34 significantly expanded gene families (SEGFs) were detected in cervids (Figure 2A), with dominant enrichment in processes related to immune response and protein translation (Supplementary Table S4). Transcriptomic profiling of embryonic antler buds from sika deer (CNCB, 2025b), combined with comparative analysis against sheep (*Ovis aries*) horn bud transcriptomes (Wang et al., 2019c), identified 3 907 genes exhibiting significantly elevated expression in antler buds (Supplementary Figure S5). These genes were predominantly associated with ATP synthesis, RNA splicing, cell migration, and proliferative capacity (Supplementary Table S5). Eighteen of these antler-enriched transcripts corresponded to cervid PSGs, with annotated roles in angiogenesis, cell differentiation, lipid transport, and immune response, implicating these loci in antler origin (Supplementary Table S6). Among this subset, *DCN*, *FST*, *IGFALS*, and *LUZP2* showed pronounced expression in the *PRRX1*+ mesenchymal lineage, comprising *PRRX1*+ mesenchymal cells (PMCs), proliferative PMCs, and antler blastema progenitor cells (ABPCs) (Li et al., 2025; Qin et al., 2023) identified within the antler regeneration periosteum (Figure 2C; Supplementary Table S7). *DCN* encodes decorin, a key regulator of collagen fibrillogenesis through high-affinity interactions with extracellular matrix components (Lieveld et al., 2014). A cervid-specific positively selected substitution was detected at amino acid position 67 (K67A; posterior probability=0.953), proximal to the leucine-rich repeat N-terminal domain, accompanied by a lineage-specific structural variant spanning residues 39–50 (Figure 2D). These alterations may modify decorin-mediated matrix organization, a process integral to tissue remodeling and regeneration (Goetsch & Niesler, 2016). *FST* encodes follistatin, a known promoter of bone regeneration through inhibition of myostatin (MSTN)-driven osteoclastogenesis (Tang et al., 2020; Wallner et al., 2017). Both *IGFALS* and *LUZP2* contribute to organ growth and developmental regulation through growth factor stabilization and cytoskeletal signaling pathways (Domené et al., 2004; Rao et al., 2023). The convergence of cervid-specific sequence evolution with elevated expression in antlerogenic tissues highlights these four genes as central components of the molecular network governing antler formation and regeneration. Their coordinated involvement in extracellular matrix dynamics, skeletal remodeling, and proliferative control underscores their relevance as priority targets for future mechanistic studies of mammalian organ regeneration.

The high-quality genome assembly of the Chinese water deer provides a powerful framework for exploring the genetic basis of antler formation from the perspective of secondary trait loss. By focusing on antler absence, 40 genes exhibiting complete loss and 188 genes showing signatures of relaxed selection (GRSs) were identified in the antlerless Chinese water deer. Among the lost genes, six loci (*TMPRSS5*, *ZNF550*, *TIGD7*, *EFCC1*, *RXFP2*, and *RADX*) were highly expressed in sika deer antler buds, with *RXFP2* and *RADX* also showing high expression in the periosteum during antler regeneration (Supplementary Table S8). Previous studies have reported convergent pseudogenization of *RXFP2* associated with antler loss in the Chinese water deer and forest musk deer (*Moschus chrysogaster* and *Moschus leucogaster*) (Wang et al., 2019c), a pattern further corroborated by the present analysis. Moreover, 31 GRSs in the Chinese water deer were highly expressed in sika deer antler buds and were significantly enriched in biological processes involving protein autophosphorylation, calcium ion transport, cell motility, and immune response (Supplementary Table S9). Functional enrichment analyses revealed that genes lost in the Chinese water deer were predominantly associated with cytidine-to-uridine RNA editing, while GRSs were primarily enriched in the calcium ion transmembrane transport into the cytosol (Figure 2E; Supplementary Table S10).

Evolutionary modulation of male secondary traits offers a valuable opportunity to dissect the genetic mechanisms shaping sexually selected traits under the influence of both sexual and natural selection pressures (Hine et al., 2011). Given the hypothesis that antler elaboration has been subject to intensified selection (Mittell et al., 2024), genetic changes were further examined in Cervini and Odocoileini, two tribes characterized by pronounced antler morphology. This analysis identified 47 PSGs in Cervini and 118 PSGs in Odocoileini, along with tribe-specific significantly expanded gene families. GO enrichment analysis revealed that PSGs in Cervini were primarily associated with regulation of hormone secretion and the MAPK signaling pathway (Figure 2E; Supplementary Table S11), whereas SEGFs in this tribe were enriched in protein translation and immune-related processes (Supplementary Table S12). The Odocoileini PSGs were enriched in RNA catabolic processes, positive regulation of B cell activation, and chondroitin sulfate proteoglycan biosynthesis (Figure 2E; Supplementary Table S13), while SEGFs showed marked enrichment in processes related to calcium ion transport and enzyme activity regulation (Supplementary Table S14).

Comparative analysis of PSCs across Cervidae, Cervini, and Odocoileini revealed a striking lack of overlap among these gene sets (Supplementary Figure S6), indicating that distinct genetic targets were under selection during different phases of cervid evolutionary history. No evidence was detected for individual genes undergoing continuous positive selection across lineages, in contrast to patterns reported for shared targets of selection in Homininae and Ponginae (Bakewell et al., 2007). This disparity likely reflects the greater diversity of phenotypic trajectories among cervids and supports the view that antler elaboration in Cervini and Odocoileini evolved through independent evolutionary routes.

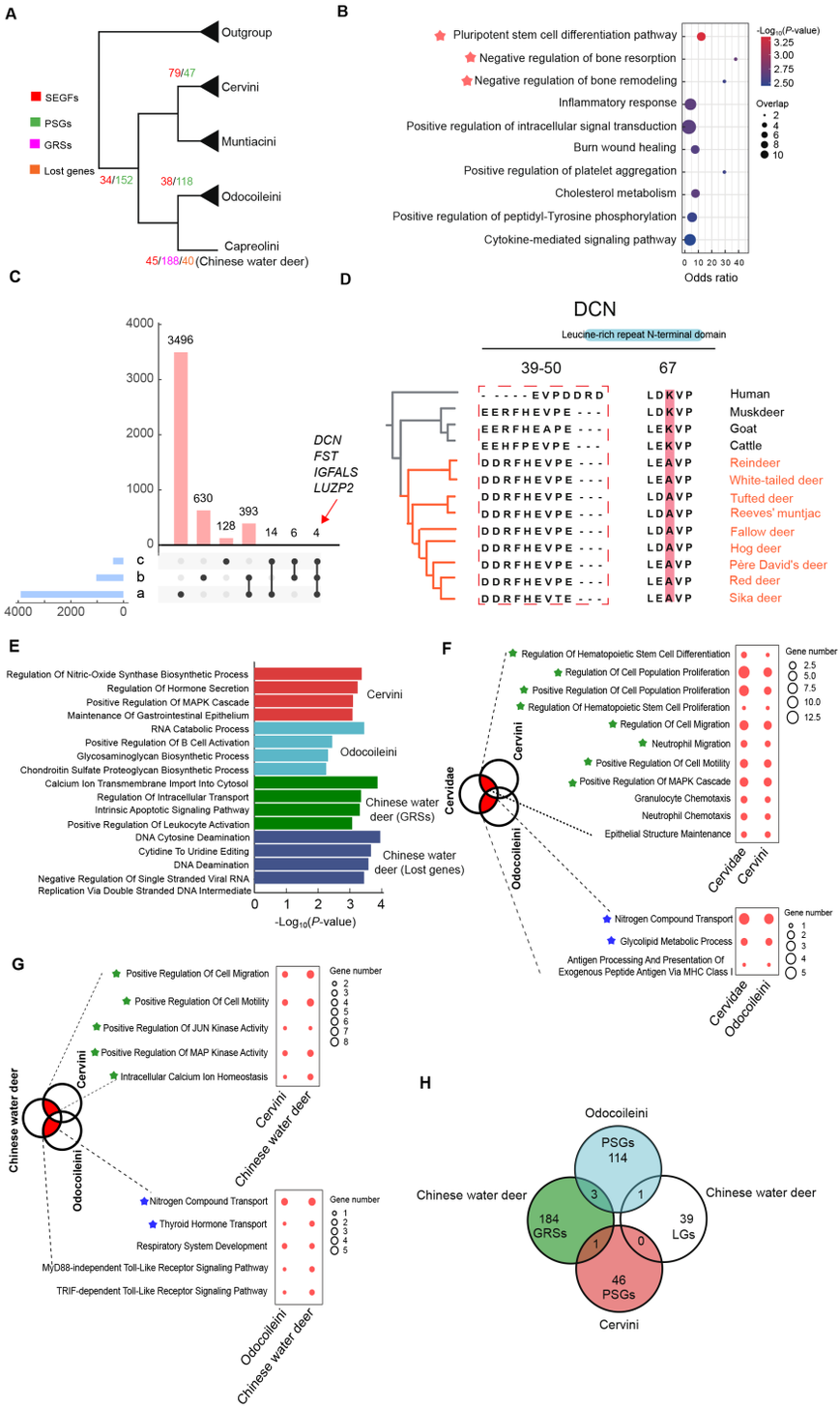

Figure 2 Genes associated with the origin and evolution of deer antlers

A: Distribution of genes under different selective regimes mapped onto the cervid phylogeny, including positively selected genes (PSGs; green), significantly expanded gene families (SEGFs; red), genes under relaxed selection (GRSs; purple; Chinese water deer), and genes lost (orange; Chinese water deer). B: Gene Ontology (GO) enrichment analysis of cervid-shared PSGs after exclusion of Chinese water deer. Red stars represent antler regeneration-related processes. C: UpSet plot of highly differentially expressed genes in antlers, highly expressed genes in PMC lineage, and Cervidae PSGs. Numbers above columns represent number of genes. (a) Highly expressed genes in antler buds; (b) Highly expressed genes in PMCs lineage; (c) Cervidae PSGs. D: *DCN* was identified as a PSG in cervids within the extracellular matrix remodeling pathway. Positively selected sites inferred for the Cervidae ancestral lineage are indicated by red bars and the structural variant is highlighted by a red dashed box. Cervid species are highlighted in orange. E: Top four significantly enriched GO processes associated with PSGs in Cervini and Odocoileini, as well as GRSs and lost genes in Chinese water deer. F: GO biological processes shared between Cervidae and Cervini/Odocoileini. G: GO biological processes shared between Chinese water deer and Cervini/Odocoileini. Shared processes are represented by green and blue stars. H: Venn diagram depicting overlap among Chinese water deer GRSs and lost genes, Cervini PSGs, and Odocoileini PSGs. Numbers within circles represent number of genes.

Despite the absence of shared genes, functional convergence emerged at the pathway level. PSGs identified at the Cervidae level and within Cervini were both significantly enriched in GO terms related to cell differentiation, proliferation, migration, and regulation of organ size, with strong involvement of the MAPK signaling pathway (Figure 2F). Notably, enrichment profiles of Cervini PSGs and GRSs in the Chinese water deer overlapped in processes related to cell migration, regulation of organ size, and calcium ion homeostasis (Figure 2G). These biological functions closely mirror cellular strategies employed by antlerogenic periosteum cells during antler formation and growth (Goss & Powel, 1985; Li & Suttie, 2000), suggesting mechanistic continuity between antler origin and subsequent enhancement within Cervini. In Odocoileini, enrichment patterns differed in emphasis. PSGs at both the Cervidae and Odocoileini levels, as well as GRSs in the Chinese water deer, were significantly enriched in processes related to transport and metabolism of nitrogen-containing compounds (Figure 2F, G). This pattern implicates nutrient uptake and metabolic regulation as important contributors to antler enhancement in Odocoileini, consistent with experimental evidence showing that nutritional restriction modulates metabolic activity through effects on organ growth in sheep (Burrin et al., 1990).

Pathway-level inspection further highlighted recurrent involvement of the RAS/MAPK signaling network. Five Cervidae PSGs associated with regulation of organ size were mapped to this pathway (Supplementary Figure S7). Additional components included *FLT4* and *MAP4K4* among Cervini PSGs, *RALGAPA2* and *PLA2G4B* among Odocoileini PSGs, and six lost genes or GRSs in the Chinese water deer (Supplementary Figure S7). These findings indicate sustained selective pressure on the RAS/MAPK pathway across cervid lineages, despite lineage-specific turnover in the underlying genes. Integration of gene expression data reinforced this conclusion. Quantification of PSG expression across antler cell populations revealed enrichment of proliferation-related pathways in Cervidae, Cervini, and Odocoileini, whereas differentiation-related pathways were preferentially enriched in Cervidae and Odocoileini (Supplementary Figure S8A, B). Targeting of different genetic components within shared regulatory pathways likely facilitated lineage-specific trajectories of antler elaboration. Collectively, these results suggest that antler evolution relied on recurrent selection acting on conserved developmental and metabolic pathways, particularly those governing cell proliferation, differentiation, and RAS/MAPK signaling, rather than on persistent selection of identical genes. Genes evolving under altered selection pressure across tribe-level lineages were examined by comparing the PSGs in Cervini and Odocoileini with genes lost or under relaxed selection in the Chinese water deer. This comparison identified *TEX51* as a gene under relaxed selection in the Chinese water deer but subject to positive selection in Cervini (Figure 2H). Previous studies have demonstrated a significant association between genetic variation at this locus and population-level differences in bone density (He et al., 2023). Within Odocoileini, three PSGs (*SMCHD1*, *MS4A8*, and *STRC*) exhibited relaxed selection in the Chinese water deer, while one Odocoileini PSG (*SLC18A1*) was completely absent from the Chinese water deer genome (Figure 2H). Functional annotation indicates involvement of *SMCHD1* in bone development (Benetti et al., 2022), *MS4A8* in the regulation of smooth muscle function within the gastrointestinal tract of mice (Ishibashi et al., 2001), and *SLC18A1* in monoamine transport into synaptic vesicles (Wimalasena, 2011).

Cancer resistance and bone metabolic remodeling in cervids associated with rapid antler growth

Antler regeneration in cervids proceeds at exceptional rates, accompanied by transient activation of proto-oncogenes and coordinated induction of tumor suppressor pathways. Prior analyses have suggested that widespread anticancer capacity in these species may result from strong selection on tumor suppressor genes (Wang et al., 2019c), reinforced by recent functional data (Rossetti et al., 2024). To further delineate the genetic mechanisms underlying the balance between rapid antler growth and cancer resistance, the present study incorporated comparative data from species bearing either hypertrophied or vestigial antlers, including taxa with antlers less than 2 cm in length (Hooijer & Granger, 1951), to evaluate potential correlations between antler morphology and tumor-suppressive adaptations.

Four PSGs implicated in apoptosis and DNA repair were newly identified in Cervidae: *TP53*, *KLK10*, *HINFP*, and *CD226* (Figure 3A). Evolutionary rate analysis across tribes revealed no significant associations between antler size and divergence patterns for these loci (Supplementary Table S15). Nevertheless, the inclusion of additional cervid genomes enabled robust classification of *TP53* as a PSG, which has not been recognized previously (Wang et al., 2019c). Sequence-level analysis showed that sites under positive selection (posterior probability>0.8) were concentrated in the DNA-binding domain of TP53 (Balagurumoorthy et al., 1995), with fixed substitutions across cervid lineages (Figure 3B). Structural modeling further demonstrated that these substitutions occurred in or near α-helical motifs. A threonine-to-isoleucine replacement in the helix core led to diminished hydrogen bonding capacity, while a second mutation involving a serine residue outside the α-helix—normally forming strong hydrogen bonds—also converted to isoleucine. These alterations are predicted to modify protein-DNA interactions and downstream regulatory effects (Supplementary Figure S9A–D). Functional characterization of the remaining three PSGs reinforces their role in tumor suppression. *KLK10* inhibits tumorigenesis in nude mice (Goyal et al., 1998) and suppresses proliferation of human esophageal cancer cells (Li et al., 2015). *HINFP* plays a critical role in maintaining genomic stability, with its deletion linked to cancer development (Nirala et al., 2021). *CD226* encodes a cell surface receptor essential for mediating antitumor immune responses (Bi, 2022).

Eleven PSGs in Cervidae were associated with pathways governing tissue regeneration and tumor suppression, including growth factor signaling, Wnt pathway activation, extracellular matrix remodeling, and regulation of stem cell properties. Among these, *NT5E*, a mesenchymal stem cell marker in both humans and mice, enhances stemness properties and regenerative capacity (Kimura et al., 2021). *FZD6*, a typical G protein-coupled receptor mediating Wnt signaling, regulates cell division, proliferation, adhesion, and migration (Beghini & Postorino, 2019; Zou et al., 2017) and displayed significant positive selection across cervid lineages (Figure 3C). Compared to the outgroup, three sites under positive selection were identified, including A465V, located

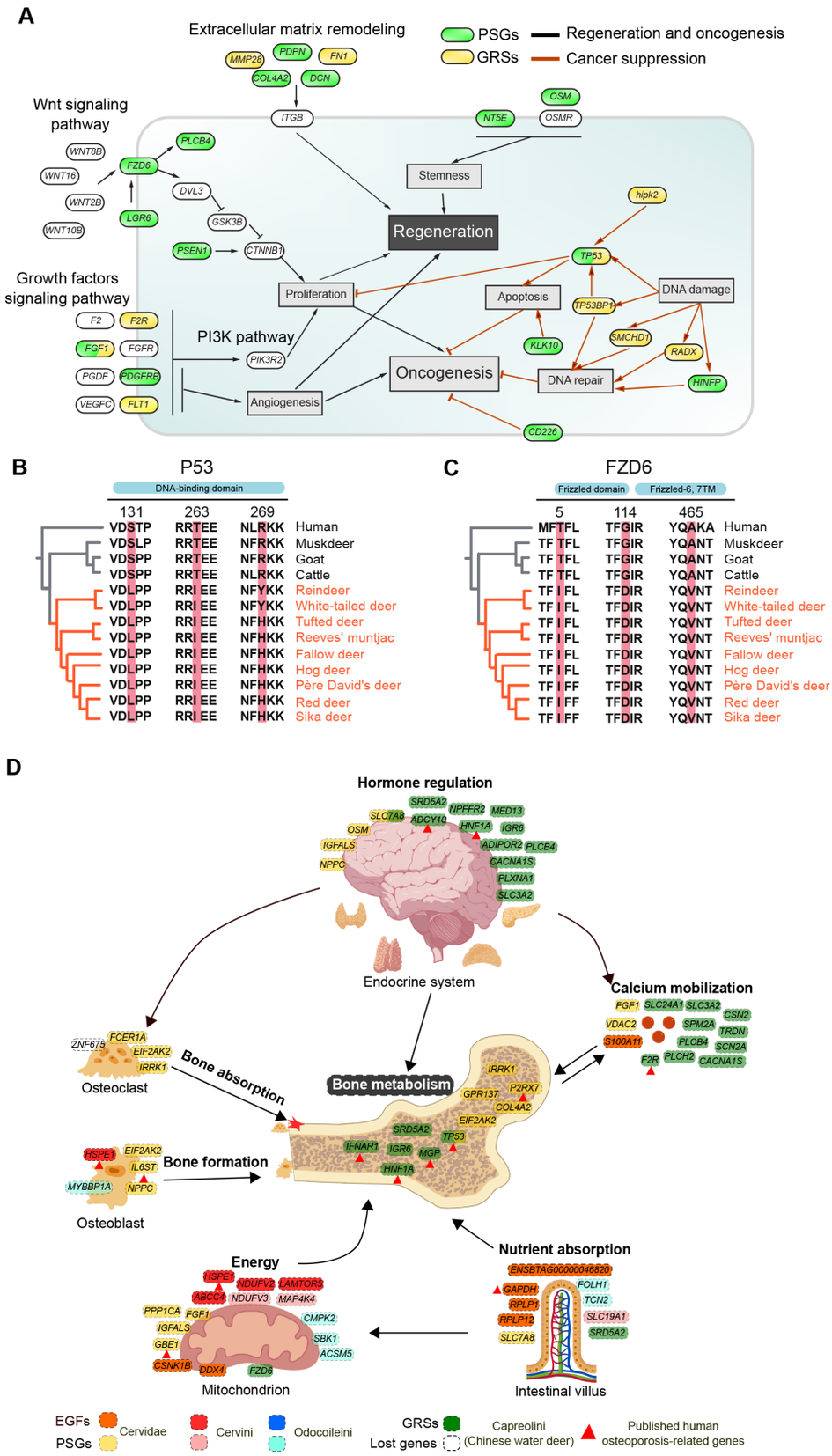

Figure 3 Co-evolution of cancer resistance and cyclic physiological osteoporosis during antler growth in cervids

A: Regulatory pathways linking rapid antler regeneration with cancer suppression, highlighting PSGs in Cervidae and GRSs in Chinese water deer. B: *TP53* was identified as under significant positive selection in the Cervidae lineage, with three positively selected sites at amino acid positions 131, 263, and 269 (indicated by red bars). C: *FZD6* was identified as a positively selected component of the Wnt signaling pathway in cervids, with positively selected sites highlighted by red bars. Cervid species in B and C are highlighted in orange. D: Evolutionary landscape of genes related to bone metabolism. Central pathways are surrounded by lineage-specific evolutionary patterns. Genes from Cervidae, Cervini, Odocoileini, and Chinese water deer are denoted by frames colored in orange, red, blue, and green, respectively. PSGs: Positively selected genes; SEGFs: Significantly expanded gene families; GRSs: Genes under relaxed selection in Chinese water deer (Capreolini).

within the ligand-binding interface of the FZD6 protein (Kozielewicz et al., 2020). A mutation at this site may alter pathway activation, suggesting that changes in *FZD6* may have contributed to the evolution of antler regenerative capacity. Intriguingly, the T5I substitution in FZD6 was located within the transmembrane α-helix, where reduced hydrogen bonding potential in cervids suggests altered molecular interaction dynamics (Supplementary Figure S9E–H). None of the genes lost in the Chinese water deer exhibited evidence of positive selection in other cervids; however, 15 genes under relaxed selection in water deer showed selective signatures in other cervids. These genes were functionally related to immune regulation, transcriptional regulation, and metabolic homeostasis (Supplementary Table S16), including *TP53* and *FGF1*, both associated with regeneration and tumor suppression (Figure 3A). *FGF1*, a member of the fibroblast growth factor family, plays a crucial role in differentiation and tissue regeneration (Conte et al., 2009). Additionally, several genes involved in growth factor signaling (*F2R* and *FLT1*), extracellular matrix remodeling (*MMP28* and *FN1*), and tumor suppressor pathways (*HIPK2*, *TP53BP1*, *SMCHD1*, and *RADX*) displayed relaxed selection in the Chinese water deer. These patterns indicate that degeneration of antlers in this lineage coincided with gradual uncoupling of regenerative and tumor-suppressive constraints. Collectively, these findings deepen understanding of how the trade-off between regeneration and cancer resistance has been differentially shaped across cervid evolution.

The annual regeneration of antlers imposes an extreme mineral demand exceeding dietary intake, which typically contains only 7%–8% calcium (Estevez et al., 2009; Muir et al., 1987). To compensate, deer undergo a profound, reversible form of skeletal demineralization termed cyclic physiological osteoporosis (CPO), characterized by seasonal bone loss and restoration (Banks et al., 1968; Borsy et al., 2009; Estevez et al., 2009; Stéger et al., 2010). In this study, analysis of Cervidae PSGs revealed several genes involved in bone remodeling and mineral homeostasis, including *GPR137*, *COL4A2*, *EIF2AK2*, *IRRK1*, and *P2RX7*, all associated with bone resorption, turnover, and mineralization (Figure 3D). Twelve additional PSGs were distributed across functional categories related to hormone-mediated bone regulation (*NPPC*, *IGFALS*, *OSM*, and *SLC7A8*), calcium mobilization (*FGF1* and *VDAC2*), osteoblast activation (*EIF2AK2*, *IL6ST*, and *NPPC*), osteoclast activation (*FCER1A*, *EIF2AK2*, and *IRRK1*), energy utilization (*PPP1CA*, *FGF1*, *IGFALS*, and *GBE1*), and nutrient absorption (*SLC7A8*) (Figure 3D). Interestingly, loss of *ZNF675*, a known suppressor of osteoclast-mediated bone resorption (Shin et al., 2002), in the Chinese water deer further suggested that these genes may be linked to the unique systemic bone metabolism capabilities of antlered cervids (Figure 3D). Several water deer GRSs were associated with bone metabolism, hormone regulation, calcium mobilization, energy metabolism, and nutrient absorption pathways, including 12 GRSs linked to bone metabolism and associated hormonal regulation and 10 GRSs linked to calcium mobilization (Figure 3D). Genes involved in vitamin absorption pathways (Benoit et al., 2021; Ganapathy et al., 2004; Guo et al., 2013) also showed lineage-specific selection, including *SLC19A1* in Cervini and *FOLH1* and *TCN2* in Odocoileini, suggesting that enhanced vitamin absorption constitutes an adaptive requirement for rapid antlerogenesis. Comparative analysis of bone metabolism regulators with a curated list of 1 499 human osteoporosis-related genes (Wang et al., 2019b) revealed four overlapping loci under positive selection in Cervidae: *TP53* and *P2RX7*, related to bone metabolism, *IL6ST*, involved in bone formation, and *GBE1*, associated with energy utilization (Figure 3D). In contrast, three osteoporosis-related genes exhibited relaxed selection in the Chinese water deer, including *ADCY10* and *HNF1A*, related to hormone regulation, and *F2R*, implicated in calcium regulation. These evolutionary patterns point to functionally relevant divergence in skeletal regulation, with potential translational value for understanding antler-associated bone physiology. The identified genes constitute a targeted resource for future investigations into the molecular basis of cyclic physiological osteoporosis, a reversible state of skeletal demineralization that remains poorly understood.

Collectively, the emergence of antlers in cervids appears to have driven extensive physiological remodeling across multiple systems, including somatic regeneration, cyclic physiological osteoporosis, mineral and vitamin metabolism, and oncogenic control. These findings underscore the relevance of deer as a powerful biomedical model for studying large-scale tissue regeneration and systemic homeostatic adaptations.

CONCLUSION

Comparative genomic analyses across cervid lineages revealed lineage-specific genomic variations associated with antler evolution and related physiological traits. Notably, convergence was observed at the pathway level, particularly in bone metabolism, rather than at the gene level, suggesting shared selective pressures shaping antler enhancement in Cervini and Odocoileini. This study presents a robust analytical framework for elucidating the evolutionary origins of lineage-specific traits in cervids, paving the way for future studies on antler regeneration, reduced oncogenic risk, and cyclic physiological osteoporosis reversal, with translational potential for biomedical applications.

DATA AVAILABILITY

All raw sequencing data generated in this study were submitted to the Genome Sequence Archive of China National Center for Bioinformation (GSA; https://ngdc.cncb.ac.cn/gsa) under accession numbers CRA022343 (genomic data) and CRA022995 (single-cell RNA-seq data). The genome assembles generated in this study were deposited in the Zenodo repository (https://doi.org/10.5281/zenodo.15594434), NCBI database (BioProjectID PRJNA1330408), and Science Data Bank (https://www.scidb.cn/s/FRRfiu).

SUPPLEMENTARY DATA

Supplementary data to this article can be found online.

COMPETING INTERESTS

The authors declare that they have no competing interests.

AUTHORS' CONTRIBUTIONS

Z.Y.Z., Z.H.L., Z.L.Z., Q.M.Z., Z.P.L., and B.W. contributed equally to this work. L.S.L., W.W., and R.H. conceived the study. Z.Y.Z., L.S.L., Q.Y.G., Z.L.Z., Q.M.Z., Z.P.L., J.M., H.S.Y., Y.S.W., G.F.Z., and Z.B.C collected the samples. Z.H.L. and L.S.L. performed the bioinformatic analyses. W.B.Z. performed data curation. Z.Y.Z., Z.H.L., Z.L.Z., Q.M.Z., Z.P.L., and L.S.L. wrote the manuscript. Z.Y.Z., Z.H.L., B.W., B.T.Z., L.S.L., M.V.W., and Q.Q. discussed the results. B.W., G.H., L.C., M.V.W., R.H., L.S.L., and W.W. revised the manuscript. All authors contributed to the data interpretation. All authors read and approved the final version of the manuscript.

ACKNOWLEDGMENTS

We thank Pan Zhang and Yun-Fang Shan from the Beijing Milu Ecological Research Center for support in sample collection and preparation. We thank Kun Wang, Yong-Xin Li, Tong-Tong Zhang, Chen-Guang Feng, and Hao-Rong Li from the School of Ecology and Environment, Northwestern Polytechnical University, for comments on an earlier draft.

REFERENCES

Armstrong J, Hickey G, Diekhans M, et al. 2020. Progressive Cactus is a multiple-genome aligner for the thousand-genome era. *Nature*, **587**(7833): 246–251.

Baker KH, Gray HWI, Ramovs V, et al. 2017. Strong population structure in a species manipulated by humans since the Neolithic: the European fallow deer (*Dama dama dama*). *Heredity*, **119**(1): 16–26.

Bakewell MA, Shi P, Zhang JZ. 2007. More genes underwent positive selection in chimpanzee evolution than in human evolution. *Proceedings of the National Academy of Sciences of the United States of America*, **104**(18): 7489–7494.

Balagurumoorthy P, Sakamoto H, Lewis MS, et al. 1995. Four p53 DNA-binding domain peptides bind natural p53-response elements and bend the DNA. *Proceedings of the National Academy of Sciences of the United States of America*, **92**(19): 8591–8595.

Bandi V, Gutwin C. 2020. Interactive exploration of genomic conservation. In: Proceedings of the 46th Graphics Interface Conference. Toronto: Canadian Human-Computer Communications Society.

Banks WJ Jr, Epling GP, Kainer RA, et al. 1968. Antler growth and osteoporosis II. Gravimetric and chemical changes in the costal compacta during the antler growth cycle. *The Anatomical Record*, **162**(4): 399–405.

Barnard RK, Smith JA, Yuan N, et al. 2023. An announcement of a new genome sequence available for *Dama dama* (fallow deer). *Forensic Science International: Animals and Environments*, **4**: 100074.

Beghini A, Postorino G. 2019. FZD6 (Frizzled class receptor 6). *Atlas of Genetics and Cytogenetics in Oncology and Haematology*, **23**(5): 112–119.

Benetti N, Gouil Q, Tapia Del Fierro A, et al. 2022. Maternal SMCHD1 regulates *Hox* gene expression and patterning in the mouse embryo. *Nature Communications*, **13**(1): 4295.

Benoit CR, Walsh DJ, Mekerishvili L, et al. 2021. Loss of the vitamin B-12 transport protein Tcn2 results in maternally inherited growth and developmental defects in zebrafish. *The Journal of Nutrition*, **151**(9): 2522–2532.

Bi JC. 2022. CD226: a potent driver of antitumor immunity that needs to be maintained. *Cellular & Molecular Immunology*, **19**(9): 969–970.

Bickhart DM, Rosen BD, Koren S, et al. 2017. Single-molecule sequencing and chromatin conformation capture enable *de novo* reference assembly of the domestic goat genome. *Nature Genetics*, **49**(4): 643–650.

Borsy A, Podani J, Stéger V, et al. 2009. Identifying novel genes involved in both deer physiological and human pathological osteoporosis. *Molecular Genetics and Genomics*, **281**(3): 301–313.

Burrin DG, Ferrell CL, Britton RA, et al. 1990. Level of nutrition and visceral organ size and metabolic activity in sheep. *British Journal of Nutrition*, **64**(2): 439–448.

Camacho C, Coulouris G, Avagyan V, et al. 2009. BLAST+: architecture and applications. *BMC Bioinformatics*, **10**(1): 421.

Cao X, Jiang H, Zhang X. 2005. Polymorphic karyotypes and sex chromosomes in the tufted deer (*Elaphodus cephalophus*): cytogenetic studies and analyses of sex chromosome-linked genes. *Cytogenetic and Genome Research*, **109**(4): 512–518.

Capella-Gutiérrez S, Silla-Martínez JM, Gabaldón T. 2009. trimAl: a tool for automated alignment trimming in large-scale phylogenetic analyses. *Bioinformatics*, **25**(15): 1972–1973.

Cegielski M, Calkosinski I, Dziegiel P, et al. 2006. Search for stem cells in the growing antler stag (*Cervus elaphus*). *Bulletin of the Veterinary Institute in Pulawy*, **50**(2): 247–251.

Chen CY, Yin Y, Li HR, et al. 2022. Ruminant-specific genes identified using high-quality genome data and their roles in rumen evolution. *Science Bulletin*, **67**(8): 825–835.

Chen EY, Tan CM, Kou Y, et al. 2013. Enrichr: interactive and collaborative HTML5 gene list enrichment analysis tool. *BMC Bioinformatics*, **14**(1): 128.

Chen L, Qiu Q, Jiang Y, et al. 2019. Large-scale ruminant genome sequencing provides insights into their evolution and distinct traits. *Science*, **364**(6446): eaav6202.

Chen SF, Zhou YQ, Chen YR, et al. 2018. fastp: an ultra-fast all-in-one FASTQ preprocessor. *Bioinformatics*, **34**(17): i884–i890.

Clutton-Brock TH, Albon SD, Guinness FE. 1988. Reproductive success in male and female red deer. *In*: Clutton-Brock TH. Reproductive Success. Chicago: University of Chicago Press.

Clutton-Brock TH, Guinness FE, Albon SD. 1982. Red Deer: Behavior and Ecology of Two Sexes. Edinburgh: Edinburgh University Press.

CNCB. 2025a. Genomic sequencing data of cervids. https://ngdc.cncb.ac.cn/gsa/search?searchTerm=CRA022343.

CNCB. 2025b. Single-cell rna sequencing of sika deer fetal antler bud. https://ngdc.cncb.ac.cn/gsa/search?searchTerm=CRA022995.

Conte C, Ainaoui N, Delluc-Clavières A, et al. 2009. Fibroblast growth factor 1 induced during myogenesis by a transcription-translation coupling mechanism. *Nucleic Acids Research*, **37**(16): 5267–5278.

Dainat J. 2022. AGAT: another gff analysis toolkit to handle annotations in any GTF/GFF format. *Zenodo*.

Danecek P, Bonfield JK, Liddle J, et al. 2021. Twelve years of SAMtools and BCFtools. *Gigascience*, **10**(2): giab008.

De Bie T, Cristianini N, Demuth JP, et al. 2006. CAFE: a computational tool for the study of gene family evolution. *Bioinformatics*, **22**(10): 1269–1271.

Domené HM, Bengolea SV, Martínez AS, et al. 2004. Deficiency of the circulating insulin-like growth factor system associated with inactivation of the acid-labile subunit gene. *New England Journal of Medicine*, **350**(6): 570–577.

Dudchenko O, Batra SS, Omer AD, et al. 2017. De novo assembly of the *Aedes aegypti* genome using Hi-C yields chromosome-length scaffolds. *Science*, **356**(6333): 92–95.

Durand NC, Shamim MS, Machol I, et al. 2016. Juicer provides a one-click system for analyzing loop-resolution Hi-C experiments. *Cell Systems*, **3**(1): 95–98.

Edgar RC. 2004. MUSCLE: multiple sequence alignment with high accuracy and high throughput. *Nucleic Acids Research*, **32**(5): 1792–1797.

Eichler EE, Sankoff D. 2003. Structural dynamics of eukaryotic chromosome evolution. *Science*, **301**(5634): 793–797.

Emms DM, Kelly S. 2019. OrthoFinder: phylogenetic orthology inference for comparative genomics. *Genome Biology*, **20**(1): 238.

Estevez JA, Landete-Castillejos T, Martínez A, et al. 2009. Antler mineral composition of Iberian red deer *Cervus elaphus hispanicus* is related to mineral profile of diet. *Acta Theriologica*, **54**(3): 235–242.

Feng SH, Bai M, Rivas-González I, et al. 2022. Incomplete lineage sorting and phenotypic evolution in marsupials. *Cell*, **185**(10): 1646**–**1660. e18.

Ganapathy V, Smith SB, Prasad PD. 2004. SLC19: the folate/thiamine transporter family. *Pflügers Archiv*, **447**(5): 641–646.

Gilbert C, Ropiquet A, Hassanin A. 2006. Mitochondrial and nuclear phylogenies of Cervidae (Mammalia, Ruminantia): systematics, morphology, and biogeography. *Molecular Phylogenetics and Evolution*, **40**(1): 101–117.

Goenka SD, Turakhia Y, Paten B, et al. 2020. SegAlign: a scalable GPU-based whole genome aligner. *In*: Proceedings of the International Conference for High Performance Computing, Networking, Storage and Analysis. Atlanta: IEEE, 1**–**13.

Goetsch KP, Niesler CU. 2016. The extracellular matrix regulates the effect of decorin and transforming growth factor beta-2 (TGF-β2) on myoblast migration. *Biochemical and Biophysical Research Communications*, **479**(2): 351–357.

Goss RJ. 1983. Deer Antlers: Regeneration, Function and Evolution. New York: Academic Press.

Goss RJ, Powel RS. 1985. Induction of deer antlers by transplanted periosteum I. Graft size and shape. *Journal of Experimental Zoology*,

235(3): 359–373.
Goyal J, Smith KM, Cowan JM, et al. 1998. The role for NES1 serine protease as a novel tumor suppressor. *Cancer Research*, **58**(21): 4782–4786.
Guo J, Xie H, Wang JH, et al. 2013. The maternal folate hydrolase gene polymorphism is associated with neural tube defects in a high-risk Chinese population. *Genes & Nutrition*, **8**(2): 191–197.
Han RB, Han L, Zhao XW, et al. 2023. Haplotype-resolved genome of sika deer reveals allele-specific gene expression and chromosome evolution. *Genomics, Proteomics & Bioinformatics*, **21**(3): 470**–**482.
Hartmann N, Scherthan H. 2004. Characterization of ancestral chromosome fusion points in the Indian muntjac deer. *Chromosoma*, **112**(5): 213–220.
He D, Liu H, Wei WM, et al. 2023. A longitudinal genome-wide association study of bone mineral density mean and variability in the UK Biobank. *Osteoporosis International*, **34**(11): 1907–1916.
Hickey G, Paten B, Earl D, et al. 2013. HAL: a hierarchical format for storing and analyzing multiple genome alignments. *Bioinformatics*, **29**(10): 1341–1342.
Hine E, McGuigan K, Blows MW. 2011. Natural selection stops the evolution of male attractiveness. *Proceedings of the National Academy of Sciences of the United States of America*, **108**(9): 3659–3664.
Hoffmann GS, Johannesen J, Griebeler EM. 2016. Population dynamics of a natural red deer population over 200 years detected via substantial changes of genetic variation. *Ecology and Evolution*, **6**(10): 3146–3153.
Hooijer DA, Granger W. 1951. Two New Deer from the Pleistocene of Wanhsien, Szechwan, China. New York: American Museum of Natural History.
Huang L, Chi JX, Nie WH, et al. 2006. Phylogenomics of several deer species revealed by comparative chromosome painting with Chinese muntjac paints. *Genetica*, **127**(1-3): 25–33.
Huybers P, Wunsch C. 2005. Obliquity pacing of the late Pleistocene glacial terminations. *Nature*, **434**(7032): 491–494.
Ishibashi K, Suzuki M, Sasaki S, et al. 2001. Identification of a new multigene four-transmembrane family (MS4A) related to CD20, HTm4 and β subunit of the high-affinity IgE receptor. *Gene*, **264**(1): 87–93.
Jiang LC, Zhu L, Li MQ, et al. 2023. Sequencing and characterization of the complete mitochondrial genome of tufted deer, *Elaphodus cephalophus* (Artiodactyla: Cervidae) and its phylogenetic position within the family Cervidae. *Pakistan Journal of Zoology*, **55**(5): 2019–2032.
Jiang S, Li HQ, Zhang LWY, et al. 2025. Generic Diagramming Platform (GDP): a comprehensive database of high-quality biomedical graphics. *Nucleic Acids Research*, **53**(D1): D1670–D1676.
Jumper J, Evans R, Pritzel A, et al. 2021. Highly accurate protein structure prediction with AlphaFold. *Nature*, **596**(7873): 583–589.
Kelley DR, Schatz MC, Salzberg SL. 2010. Quake: quality-aware detection and correction of sequencing errors. *Genome Biology*, **11**(11): R116.
Kimura K, Breitbach M, Schildberg FA, et al. 2021. Bone marrow CD73$^+$ mesenchymal stem cells display increased stemness *in vitro* and promote fracture healing *in vivo*. *Bone Reports*, **15**: 101133.
Kirilenko BM, Munegowda C, Osipova E, et al. 2023. Integrating gene annotation with orthology inference at scale. *Science*, **380**(6643): eabn3107.
Kolberg L, Raudvere U, Kuzmin I, et al. 2023. g: profiler-interoperable web service for functional enrichment analysis and gene identifier mapping (2023 update). *Nucleic Acids Research*, **51**(W1): W207–W212.
Kozielewicz P, Turku A, Bowin CF, et al. 2020. Structural insight into small molecule action on Frizzleds. *Nature Communications*, **11**(1): 414.
Kruuk LEB, Slate J, Pemberton JM, et al. 2002. Antler size in red deer: heritability and selection but no evolution. *Evolution*, **56**(8): 1683–1695.
Kvalnes T, Flagstad Ø, Våge J, et al. 2024. Harvest and decimation affect genetic drift and the effective population size in wild reindeer. *Evolutionary Applications*, **17**(4): e13684.
Lamb S, Taylor AM, Hughes TA, et al. 2021. *De novo* chromosome-length assembly of the mule deer (*Odocoileus hemionus*) genome. *GigaByte*, **2021**: gigabyte34.
Landete-Castillejos T, Kierdorf H, Gomez S, et al. 2019. Antlers - Evolution, development, structure, composition, and biomechanics of an outstanding type of bone. *Bone*, **128**: 115046.
Li CY, Suttie JM. 2000. Histological studies of pedicle skin formation and its transformation to antler velvet in red deer (*Cervus elaphus*). *The Anatomical Record*, **260**(1): 62–71.
Li H, Durbin R. 2011. Inference of human population history from individual whole-genome sequences. *Nature*, **475**(7357): 493–496.
Li L, Xu N, Fan N, et al. 2015. Upregulated KLK10 inhibits esophageal cancer proliferation and enhances cisplatin sensitivity *in vitro*. *Oncology Reports*, **34**(5): 2325–2332.
Li ZH, Xu ZY, Zhu L, et al. 2025. High-quality sika deer omics data and integrative analysis reveal genic and cellular regulation of antler regeneration. *Genome Research*, **35**(1): 188–201.
Lieveld M, Bodson E, De Boeck G, et al. 2014. Gene expression profiling of giant cell tumor of bone reveals downregulation of extracellular matrix components decorin and lumican associated with lung metastasis. *Virchows Archiv*, **465**(6): 703–713.
Liu C, Gao JB, Cui XX, et al. 2021. A towering genome: experimentally validated adaptations to high blood pressure and extreme stature in the giraffe. *Science Advances*, **7**(12): eabe9459.
Locke WW. 1990. Late Pleistocene glaciers and the climate of western Montana, U. S. A. *Arctic and Alpine Research*, **22**(1): 1–13.
Lombard LS, Witte EJ. 1959. Frequency and types of tumors in mammals and birds of the philadelphia zoological garden. *Cancer Research*, **19**(2): 127–141.
London EW, Roca AL, Novakofski JE, et al. 2022. A de novo chromosome-level genome assembly of the white-tailed deer, *Odocoileus virginianus*. *Journal of Heredity*, **113**(4): 479–489.
Lorenzen ED, Nogués-Bravo D, Orlando L, et al. 2011. Species-specific responses of Late Quaternary megafauna to climate and humans. *Nature*, **479**(7373): 359–364.
Love MI, Huber W, Anders S. 2014. Moderated estimation of fold change and dispersion for RNA-seq data with DESeq2. *Genome Biology*, **15**(12): 550.
Malo AF, Roldan ERS, Garde J, et al. 2005. Antlers honestly advertise sperm production and quality. *Proceedings of the Royal Society B: Biological Sciences*, **272**(1559): 149–157.
Minh BQ, Schmidt HA, Chernomor O, et al. 2020. IQ-TREE 2: new models and efficient methods for phylogenetic inference in the genomic era. *Molecular Biology and Evolution*, **37**(5): 1530–1534.
Mirdita M, Schütze K, Moriwaki Y, et al. 2022. ColabFold: making protein folding accessible to all. *Nature Methods*, **19**(6): 679–682.
Mittell EA, Mandaliya P, Pemberton JM, et al. 2024. Antler size in red deer: declining selection and increasing genetic variance with age, but little senescence. *Journal of Evolutionary Biology*, **37**(11): 1288–1297.
Muir PD, Sykes AR, Barrell GK. 1987. Calcium metabolism in red deer (*Cervus elaphus*) offered herbages during antlerogenesis: kinetic and stable balance studies. *The Journal of Agricultural Science*, **109**(2): 357–364.
Nirala NK, Li Q, Ghule PN, et al. 2021. Hinfp is a guardian of the somatic genome by repressing transposable elements. *Proceedings of the National Academy of Sciences of the United States of America*, **118**(41): e2100839118.
Paysan-Lafosse T, Blum M, Chuguransky S, et al. 2023. InterPro in 2022. *Nucleic Acids Research*, **51**(D1): D418–D427.
Pemberton J, Johnston SE, Fletcher TJ, et al. 2021. The genome sequence of the red deer, *Cervus elaphus* Linnaeus 1758. *Wellcome Open Research*, **6**: 336.
Pertea G, Pertea M. 2020. GFF utilities: GffRead and GffCompare. *F1000Research*, **9**: 304.
Pertea M, Pertea GM, Antonescu CM, et al. 2015. StringTie enables improved reconstruction of a transcriptome from RNA-seq reads. *Nature Biotechnology*, **33**(3): 290–295.
Pond SLK, Frost SDW. 2005. Datamonkey: rapid detection of selective pressure on individual sites of codon alignments. *Bioinformatics*, **21**(10):

2531–2533.
Pond SLK, Frost SDW, Muse SV. 2005. HyPhy: hypothesis testing using phylogenies. *Bioinformatics*, **21**(5): 676–679.
Price JS, Allen S, Faucheux C, et al. 2005. Deer antlers: a zoological curiosity or the key to understanding organ regeneration in mammals?. *Journal of Anatomy*, **207**(5): 603–618.
Qin T, Zhang GK, Zheng Y, et al. 2023. A population of stem cells with strong regenerative potential discovered in deer antlers. *Science*, **379**(6634): 840–847.
Rabanal FA, Gräff M, Lanz C, et al. 2022. Pushing the limits of HiFi assemblies reveals centromere diversity between two *Arabidopsis thaliana* genomes. *Nucleic Acids Research*, **50**(21): 12309–12327.
Ramsey DSL, Pacioni C, White L, et al. 2019. Abundance and population genetics of Hog deer (*Axis porcinus*) in Victoria. Heidelberg, Victoria: Department of Energy, Environment and Climate Action.
Raney BJ, Barber GP, Benet-Pagès A, et al. 2024. The UCSC Genome Browser database: 2024 update. *Nucleic Acids Research*, **52**(D1): D1082–D1088.
Ranwez V, Douzery EJP, Cambon C, et al. 2018. MACSE v2: toolkit for the alignment of coding sequences accounting for frameshifts and stop codons. *Molecular Biology and Evolution*, **35**(10): 2582–2584.
Rao L, Cai LP, Huang LS. 2023. Single-cell dynamics of liver development in postnatal pigs. *Science Bulletin*, **68**(21): 2583–2597.
Rhie A, Walenz BP, Koren S, et al. 2020. Merqury: reference-free quality, completeness, and phasing assessment for genome assemblies. *Genome Biology*, **21**(1): 245.
Rosen BD, Bickhart DM, Schnabel RD, et al. 2020. *De novo* assembly of the cattle reference genome with single-molecule sequencing. *Gigascience*, **9**(3): giaa021.
Rossetti A, Chonco L, Alegría N, et al. 2024. General direct anticancer effects of deer growing antler extract in several tumour cell lines, and immune system-mediated effects in xenograft glioblastoma. *Pharmaceutics*, **16**(5): 610.
Samejima Y, Matsuoka H. 2020. A new viewpoint on antlers reveals the evolutionary history of deer (Cervidae, Mammalia). *Scientific Reports*, **10**(1): 8910.
Sayyari E, Whitfield JB, Mirarab S. 2018. DiscoVista: interpretable visualizations of gene tree discordance. *Molecular Phylogenetics and Evolution*, **122**: 110–115.
Shao YY, Lu N, Wu ZF, et al. 2018. Creating a functional single-chromosome yeast. *Nature*, **560**(7718): 331–335.
Shin JN, Kim I, Lee JS, et al. 2002. A novel zinc finger protein that inhibits osteoclastogenesis and the function of tumor necrosis factor receptor-associated factor 6. *Journal of Biological Chemistry*, **277**(10): 8346–8353.
Smith AT, Xie Y, Hoffmann RS, et al. 2008. A Guide to the Mammals of China. Princeton: Princeton University Press, 544.
Sommer RS, Kalbe J, Ekström J, et al. 2014. Range dynamics of the reindeer in Europe during the last 25, 000 years. *Journal of Biogeography*, **41**(2): 298–306.
Stéger V, Molnár A, Borsy A, et al. 2010. Antler development and coupled osteoporosis in the skeleton of red deer *Cervus elaphus*: expression dynamics for regulatory and effector genes. *Molecular Genetics and Genomics*, **284**(4): 273–287.
Sun ZL, Pan T, Wang H, et al. 2016. Yangtze River, an insignificant genetic boundary in tufted deer (*Elaphodus cephalophus*): the evidence from a first population genetics study. *PeerJ*, **4**: e2654.
Suttie JM. 1980. The effect of antler removal on dominance and fighting behaviour in farmed red deer stags. *Journal of Zoology*, **190**(2): 217–224.
Tang RH, Harasymowicz NS, Wu CL, et al. 2020. Gene therapy for follistatin mitigates systemic metabolic inflammation and post-traumatic arthritis in high-fat diet-induced obesity. *Science Advances*, **6**(19): eaaz7492.
Tarailo-Graovac M, Chen NS. 2009. Using RepeatMasker to identify repetitive elements in genomic sequences. *Current Protocols in Bioinformatics*, 4.10. 11**–**14.10. 14.
Wallner C, Jaurich H, Wagner JM, et al. 2017. Inhibition of GDF8 (Myostatin) accelerates bone regeneration in diabetes mellitus type 2. *Scientific Reports*, **7**(1): 9878.
Wang B, Chen L, Wang W. 2019a. Genomic insights into ruminant evolution: from past to future prospects. *Zoological Research*, **40**(6): 476–487.
Wang LB, Li ZK, Wang LY, et al. 2022. A sustainable mouse karyotype created by programmed chromosome fusion. *Science*, **377**(6609): 967–975.
Wang W, Lan H. 2000. Rapid and parallel chromosomal number reductions in muntjac deer inferred from mitochondrial DNA phylogeny. *Molecular Biology and Evolution*, **17**(9): 1326–1333.
Wang X, Diao LH, Sun DZ, et al. 2019b. OsteoporosAtlas: a human osteoporosis-related gene database. *PeerJ*, **7**: e6778.
Wang Y, Zhang CZ, Wang NN, et al. 2019c. Genetic basis of ruminant headgear and rapid antler regeneration. *Science*, **364**(6446): eaav6335.
Wang YP, Tang HB, Debarry JD, et al. 2012. *MCScanX*: a toolkit for detection and evolutionary analysis of gene synteny and collinearity. *Nucleic Acids Research*, **40**(7): e49.
Waterhouse RM, Seppey M, Simão FA, et al. 2018. BUSCO applications from quality assessments to gene prediction and phylogenomics. *Molecular Biology and Evolution*, **35**(3): 543–548.
Wilson DE, Reeder DM. 1993. Mammal Species of the World: A Taxonomic and Geographic Reference. 2nd ed. Washington: Smithsonian Institution Press.
Wimalasena K. 2011. Vesicular monoamine transporters: structure-function, pharmacology, and medicinal chemistry. *Medicinal Research Reviews*, **31**(4): 483–519.
Wolf FA, Angerer P, Theis FJ. 2018. SCANPY: large-scale single-cell gene expression data analysis. *Genome Biology*, **19**(1): 15.
Wu H, Luo LY, Zhang YH, et al. 2024. Telomere-to-telomere genome assembly of a male goat reveals variants associated with cashmere traits. *Nature Communications*, **15**(1): 10041.
Xing XM, Ai C, Wang TJ, et al. 2023. The first high-quality reference genome of sika deer provides insights into high-tannin adaptation. *Genomics, Proteomics & Bioinformatics*, **21**(1): 203**–**215.
Yang F, O'Brien PCM, Wienberg J, et al. 1997. Chromosomal evolution of the Chinese muntjac (*Muntiacus reevesi*). *Chromosoma*, **106**(1): 37–43.
Yang ZH. 2007. PAML 4: phylogenetic analysis by maximum likelihood. *Molecular Biology and Evolution*, **24**(8): 1586–1591.
Yin Y, Fan HZ, Zhou BT, et al. 2021. Molecular mechanisms and topological consequences of drastic chromosomal rearrangements of muntjac deer. *Nature Communications*, **12**(1): 6858.
Zhang C, Rabiee M, Sayyari E, et al. 2018. ASTRAL-III: polynomial time species tree reconstruction from partially resolved gene trees. *BMC Bioinformatics*, **19**(6): 153.
Zhang WQ, Zhang MH. 2012. Phylogeny and evolution of Cervidae based on complete mitochondrial genomes. *Genetics and Molecular Research*, **11**(1): 628–635.
Zhang Y, Park C, Bennett C, et al. 2021a. Rapid and accurate alignment of nucleotide conversion sequencing reads with HISAT-3N. *Genome Research*, **31**(7): 1290–1295.
Zhang YC, Lwin YH, Li R, et al. 2021b. Molecular phylogeny of the genus *Muntiacus* with special emphasis on the phylogenetic position of *Muntiacus gongshanensis*. *Zoological Research*, **42**(2): 212–216.
Zou LJ, Wang XC, Jiang LP, et al. 2017. Molecular cloning, characterization and expression analysis of Frizzled 6 in the small intestine of pigs (*Sus scrofa*). *PLoS One*, **12**(6): e0179421.